Journal of
MaterialsChemistry A

ROYAL SOCIETY OF CHEMISTRY

Nitrogen Promoted Molybdenum Dioxide Nanosheets for Electrochemical Hydrogen Generation

SCHOLARONE™
Manuscripts

Journal Name

ARTICLE

Nitrogen Promoted Molybdenum Dioxide Nanosheets for Electrochemical Hydrogen Generation

Junqing Yan[a,f]†, Ling Li[c]†, Yujin Ji[b]†, Ping Li[a], Lingqiao Kong[a], Xuediao Cai[c], Youyong Li[b]*, Tianyi Ma[d]*, and Shengzhong (Frank) Liu[a,e]*

Recently, hydrogen evolution reaction (HER) from electrocatalytic water splitting offers a promising and sustainable strategy for energy conversion and storage. A cheap and efficient electrocatalyst composed of Earth-abundant elements is needed. Herein, we have synthesized a new N-MoO$_2$ sheet sample with the excellent stable Pt-like HER performance. One simple and repeatable strategy is developed via taking use of cheap, simple small organic molecule urea as the reducing agent. We confirm that the N doping can induce the disordered surface lattice and increase the proton adsorption sites with the relative weak binding force. Due to the cooperative effects of surface N doping, disordered surface distortion and also the intrinsic nature of MoO$_2$, the high and considerable HER activity can be obtained with the activity of η = 96 mV vs RHE for the current density of −10 mA·cm^{-2}, a Tafel slope of 33 mV per decade. Moreover, we further expand the synthesis method to Ni and Co systems with the N-NiO/Ni and N-CoO/Co core-shell structures formation and they presented the enhanced HER performance compared to bare MO/M (M=metal) samples. This study can help us design new Earth-abundant electrocatalysts with further enhanced catalytic performance.

1. Introduction

Hydrogen (H$_2$) is considered as one promising clean energy carrier owing to the zero carbon emission when used and a suitable candidate to substitute fossil fuels for solving the energy and environmental crisis in future. Water takes a large proportion (ca. 70%) of the earth surface. As a result, hydrogen evolution reaction (HER) from water splitting has been regarded as a significant way for large-scale producing H$_2$ and attracted a great deal of attention by researchers.[1-6] Three necessaries should be satisfied for one practical HER

electrocatalyst: good activity, corrosion resistance or stability and cost-effectiveness.[7-10] And the noble metals, such as platinum-group materials, can meet the first two requirements and be used currently. Therefore, it is highly necessary to develop new earth-abundant/ low-cost electalysts with high activity to replace Pt-based materials.[10-13] To this end, many efforts have already been made to obtain some considerable candidates using the non-noble metals, such as MoS$_2$,[10, 14] WS$_2$,[15] NiS$_2$,[16] Mo$_2$C,[17] MoN[18-20] and self-supportive electrocatalysts[21] etc. Although the comparative HER performance to Pt-group samples, there is one important disadvantage of these non-oxides: stability. The sulfide, carbide or phosphide always suffers the shortcoming of becoming oxidized after long-time HER process, leading to the activity attenuation.[22-23] The research based on oxide is needed for satisfying the three HER requirements.

Molybdenum (Mo) based materials have been emerged as a new promising earth-abundant HER catalyst.[14, 24-28] And among Mo-based oxide materials containing MoO$_3$, MoO$_{3-x}$ and MoO$_2$, the MoO$_{3-x}$ based samples give more efficient HER performance than that of MoO$_3$.[29-31] As reported that the oxygen vacancies in MoO$_3$ can not only improve the conductivity but also work as the adsorption sites.[30-31] Introducing other elements into the MoO$_{3-x}$ lattice can improve its stability and performance during the employment of HER. For the application of MoO$_{3-x}$ based HER, three issues should be considered for obtaining high and stable performance. Firstly, the catalyst should expose the suitable amount of oxygen vacancies for acting as the reaction sites and improving the proton migration rate; secondly, the

a. Key Laboratory of Applied Surface and Colloid Chemistry, Ministry of Education; Shaanxi Engineering Lab for Advanced Energy Technology, School of Materials Science and Engineering, Shaanxi Normal University, Xi'an, 710119, People's Republic of China.
E-mail: liusz@snnu.edu.cn.
b. Institute of Functional Nano & Soft Materials (FUNSOM), Jiangsu Key Laboratory for Carbon-Based Functional Materials & Devices, Soochow University, Suzhou, Jiangsu 215123, People's Republic of China. E-mail: yyli@suda.edu.cn.
c. Key Laboratory of Macromolecular Science of Shaanxi Province; Shaanxi Engineering Lab for Advanced Energy Technology, School of Chemistry and Chemical Engineering, Shaanxi Normal University, Xi'an, 710119, People's Republic of China.
d. Discipline of Chemistry, School of Environmental and Life Sciences, University of Newcastle, Callaghan, NSW, Australia, E-mail: tianyi.ma@newcastle.edu.au
e. iChEM, Dalian Institute of Chemical Physics, Dalian National Laboratory for Clean Energy, Chinese Academy of Sciences, Dalian, 116023, People's Republic of China.
f. Division of Materials and Manufacturing Science, Graduate School of Engineering, Osaka University, Osaka, 565-0871, Japan.
† These authors contributed equally to this work..
Electronic Supplementary Information (ESI) available: [details of any supplementary information available should be included here]. See DOI: 10.1039/x0xx00000x

oxidation of the surface defect sites by water or dissolved oxygen often leads to the change of phase or decline of activity; thirdly, for the Pt-like catalyst, the HER process follows the Volmer-Tafel mechanism, which contains a chemical adsorption step (eq 1) and an electron transfer step (eq 2),[16] the studied sample should expose proper vacant electron orbits for proton adsorption. To date, it is still needed to research and synthesize new MoO_{3-x} based sample to obtain the considerable results with high HER performance, good stability and Pt-like reaction pathways.

The Volmer reaction: $H^+ + e \rightarrow H_{(ads)}$ (1)

The Tafel reaction: $H_{(ads)} + H_{(ads)} \rightarrow H_2$ (2)
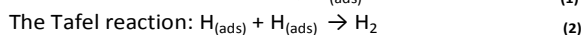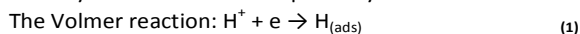
Molybdenum dioxide (MoO_2) is developed from MoO_{3-x} based samples and owns a high metallic-like electrical conductivity.[32-36] It is mentioned that MoO_2 suffers the unwelcome aggregation phenomenon when used in the HER application and also exposes a few active sites.[32] To achieve the Pt-like HER performance, the catalyst should present a fast Volmer reaction and also the Tafel step. The heteroatom (N, P, S) doping can change the surface valence state, meanwhile the unoccupied orbital of the doped heteroatom can provide the convenient for the Tafel and Volmer steps. Nitrogen (N) element owns a relative smaller radius than oxygen, and has three unpaired outer-shell electrons. As expected, replacing O atom by N atom can slightly disorder the lattice structure of one oxide, exposing one vacant orbital. Therefore, it is meaningful to design one N doped MoO_2, which could manifest a better HER performance. High-temperature nitrogen doping is one common way to synthesize N doped oxides, while it is complicated and hard to control the precursor unchanged morphology. Herein, we developed one simple, one-step and repeatable strategy to synthesize N doped MoO_2 sample by using the layered MoO_3 and urea under a relative high calcination temperature (550˚C). Especially, the obtained N-MoO_2 sample maintain the two-dimensional (2D) structure with the Pt-like HER performance.

2. Results and discussion

2.1 Synthesis and characterization of N-MoO_2 nanosheets

To begin with, layered $MoO_3 \cdot nH_2O$ with ca. 100 nm thickness as shown in Figure S1 was prepared.[37] As previously reported in the literature, the weak van der Waals' forces hold the planar double layer sheets of $MoO_3 \cdot nH_2O$, the layered structure is suitable for insertion of small ions such as H^+ or dodecylamine (DDA),[37] and also a small gas molecule with the suitable size can enter its lamellar spacing. The entered gas may induce the dissociation of layered structure or react with the distorted MoO_6 octahedra under a certain condition. In our present work, the solid-state synthetic strategy was tried to synthesize layered N-MoO_2 samples with urea working as the nitrogen source. Urea is an interesting and powerful small organic molecule with the low-cost and abundant
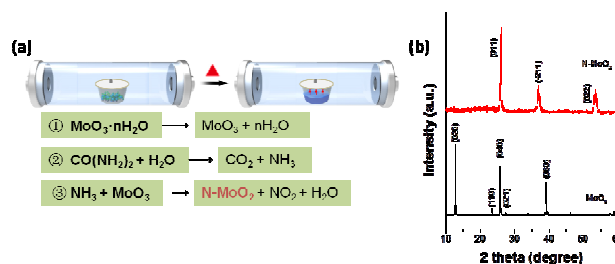
Fig. 1. (a) Schematic of the preparation of N-MoO_2 and the corresponding proposed three reaction pathways. (b) XRD patterns of N-MoO_2 and reference MoO_3 sample. The N-MoO_2 was synthesized under the below experiment conditions: the molar ratio of $MoO_3 \cdot nH_2O$ to urea is 1:2 and the calcination temperature is 550 °C under the Ar atmosphere.

characteristics. Under the low temperature, it also can easily thermal decompose into small molecule NH_3, which can be used as one reducer. For the synthesis of target material of N doped MoO_2, the $MoO_3 \cdot nH_2O$ and urea with a certain molar ratio were mixed and grinded by one mortar uniformity and thoroughly. The mixture was transferred to one crucible with one cover as shown in **Fig. 1**(a), and then they were treated at a certain temperature under the argon gas atmosphere (20 ml/min) along the possible reaction pathways. The gases was tested through TG-MS as shown in Figure S2, which clear confirmed the above proposed reactions

Fig. 1(b) presents the XRD spectra of N-MoO_2 and reference MoO_3 under study. Under the control condition of $MoO_3 \cdot nH_2O$ to urea molar ratio of 1:2 and the calcination temperature of 550 °C. Obviously, there are three peaks at 2 theta of 26°, 37° and 53.5°, which belong to the typical (011), (-211) and (022) of MoO_2 (PDF: 97-015-2316) for the N-MoO_2 sample. When changing the molar ratio to 1:1 and 1:3, the products were shown as pure (named as N-MoO_2-1) and impurity doped (named as N-MoO_2-2) MoO_2 phase (Fig. S3(a)), respectively. For the N-MoO_2-2, the impure peak loaded at 2 theta of 43.4° was attributable to (200) of cubic molybdenum nitride (3/2) (PDF: 97-004-4377). When changing the calcination temperature to 500, 600 and 650 °C, the sample with typical MoO_2 XRD peaks was first obtained and then molybdenum nitride appeared for the last two temperatures as shown in Fig. S3(b). Based on above experiments, it should be mentioned that the suitable treat temperature and molar ratio were needed for obtaining typical MoO_2 phase. As a contrast, pure $MoO_3 \cdot nH_2O$ without urea adding was treated under the same condition but the different temperature. Fig. S3(c) showed the corresponding results. Clearly, under the temperature of 550 °C, the mixture of MoO_3 and MoO_2 was obtained. For the temperature of 600 and 650 °C, pure MoO_2 was synthesized and named as MoO_2-600 and MoO_2-650, respectively. It was an interesting experimental result: pure MoO_3 could be changed into MoO_2 under the Ar gas atmosphere calcination, the adding of urea just lowered the transformation temperature. However, a low temperature maintained the morphology of the precursor. The sample of MoO_2-600 owned the similar 2-D layered structure with the close specific surface area and was used as the reference MoO_2 (named as MoO_2) sample in the below experiment.
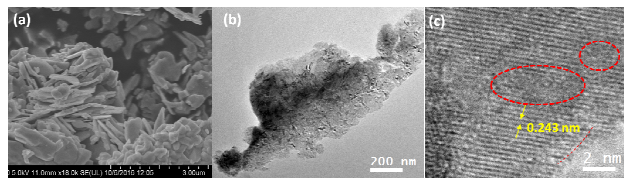
Fig. 2. Morphology characterization of N-MoO$_2$ sample. (a) SEM image, (b) TEM image and (c) HRTEM image. The disordered lattice structure in (c) is labeled by red dots.

Fig. 3. The high-resolution XPS spectrum of (a) Mo 3d, (b) O 1s and (c) N 1s of N-MoO$_2$, reference MoO$_2$ and MoO$_3$ samples under study.

The morphologies of obtained N-MoO$_2$ samples were investigated by electron microscope analysis, and the represented scanning electron microscope (SEM) and transmission electron microscope (TEM) images are shown in **Fig. 2**. Compared to the layered MoO$_3$ structure in Fig. S1, the studied N-MoO$_2$ sample also showed the 2-D sheet structure as given in **Fig. 2**(a), and the thickness could be measured ca. 30-50 nm, thinner than the fresh MoO$_3$, suggesting the developed solid-state reaction conditions could dissociate the layered structure by releasing water vapor and NH$_3$ gas entering. **Fig. 2**(b) showed the corresponding TEM image, further confirming the nanosheet structure formation of the studied N-MoO$_2$ sample. The high-resolution transmission electron microscope (HRTEM) in **Fig. 2**(c) clearly showed the lattice fringe with some obvious distortion structure at the surface sites. The interplanar crystal spacing was calculated to be ca. 0.243 nm (Fig. S4), which was assigned to (-211) facet of MoO$_2$ sample (PDF: 97-015-2316). The surface disorder of the lattice fringe was marked by red dots as shown in **Fig. 2**(c). During the reaction process, the reduction of MoO$_3$ by gas (urea or NH$_3$) was accompanied by the destroy of weak van der Waals' forces between the layers. The N element doping was then happened with the distorted surface lattices. Moreover, the atomic radius of N was smaller than O element slightly and this also could induce the above phenomenon. Fig. S5 shows the TEM images of the samples synthesized under the MoO$_3$ to urea molar ratio of 1:2 at the three temperatures of 500, 600 and 650 ℃. Typically, for the N-MoO$_2$-500, the clear nanosheet morphology can be found. Meanwhile, for the two samples of N-MoO$_2$-600 and N-MoO$_2$-650, nanoparticle appearance with the size of ca. 10 nm appears, no agglomerate bulk object can be found. Fig. S6 shows the corresponding TEM images of N-MoO$_2$-1 and N-MoO$_2$-2, synthesized under the condition of molar ratios to urea of 1:1 and 1:3. Thin and irregular layered structure can be found. The two experiments further suggested the interaction between layered MoO$_3$ and gas. Fig. S7 shows the SEM image with the corresponding element mapping of the N-MoO$_2$ sample. Clearly, only three elements of Mo, O and N can be found with the result of uniform distribution. We also tested the TEM image of reference MoO$_2$ (MoO$_2$-600) sample as given in Fig. S8, clearly showing the similar sheet to studied N-MoO$_2$.

To obtain more information about the studied samples, the surface and sub-surface states (in the depth up to ca. 5 nm) of MoO$_3$, MoO$_2$ and N-MoO$_2$ nanosheet samples are investigated by means of X-ray photoelectron spectroscopy (XPS) and the
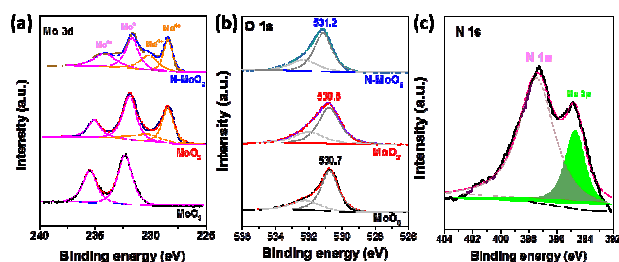
results are given in **Fig. 3**. In Mo 3d region for the three samples, different XPS peaks can be found. Typically, the Mo 3d core level spectrum of the MoO$_3$ consists of two peaks at 235.1 and 232.2 eV, which are attributed to 3d$_{3/2}$ and 3d$_{5/2}$ of the Mo^{6+}.[29-31] Meanwhile, no other valance states can be observed, suggesting the fully stoichiometric structure of the reference MoO$_3$ sample, corresponding to above XRD pattern. For the MoO$_2$ and N-MoO$_2$ samples, three peaks loaded at 235.1, 231.8 and 228.4 eV (for MoO$_2$ sample), 234.7, 231.4 and 228.3 eV (for N-MoO$_2$ sample) can be found. The first peak loaded at ca. 235 eV is assigned to Mo^{6+}, while the peaks loaded at ca. 231.5 eV and 228.3 eV can belong to Mo^{6+}/Mo^{4+} and Mo^{4+}, respectively.[32-35] For MoO$_2$-based samples, it is the inescapability of showing the Mo^{6+} signals in XPS peak.[32-35] However, for the N-MoO$_2$ sample, the Mo^{6+} peaks present the lower intensity than the MoO$_2$ and shift to low binding energy, suggesting that the N element introducing can weak the surface oxidation. To give the detailed and accurate XPS information. A series of MoO$_2$-based samples were synthesized and tested by XPS and the corresponding curves were shown in Fig. S9. With the increasing calcination temperature (from 500 to 800 ℃), the amount of surface MoO$_3$ is decreasing until disappears completely (750 and 800 ℃). Fig. S9 shows the changing situation of the three elements of Mo 3d, O 1s and N 1s with the relative correct binding energy values, which can be used to analyze the studied samples. For the O 1s condition of the MoO$_3$, MoO$_2$ and N-MoO$_2$ samples, all give one peak centered at 530.7, 530.8 and 531.2 eV, respectively. According to the Fig. S9b, we can obtain the affiliation of these peaks easily, i.e. the first belonging to O-Mo bonds of MoO$_3$ and the last belonging to the O-Mo bonds in both MoO$_2$ and MoO$_3$. It should be mentioned that the binding energy of O 1s peak of MoO$_2$ is higher than the O 1s of MoO$_3$. In the N 1s region of N-MoO$_2$ sample, two peaks can be found with the binding energy loading at 397.4 and 397.8 eV. The first peak is assigned to N 1s and the second peak belongs to Mo 3p peak (Fig. S9c).

According to above analysis, the modulating formation process of N doped MoO$_2$ based samples with different phases and morphology (Fig. S3-S6) should be clarified. To detect the pathway of the proposed gas-solid reaction between urea and MoO$_3$ (Fig. S1), in situ FTIR was carried out and the corresponding results were shown in Fig. S10 and S11. Clearly, according to Fig. S10 of the in situ FTIR study under the thermal temperature ranging from 30 ℃ to 580 ℃, the IR

curves showed the change trend, suggesting a detectable gas-solid reaction. Therefore, the IR wavenumber range from 400 to 1200 cm^{-1} was picked out to illustrate the herein designated infrared fingerprint region as shown in Fig. S11. Typically, the peak located at 670 cm^{-1} was assigned to the bending vibration of CO_2; while the peak centered at 1101 cm^{-1} belonged to stretching vibration of C-N in urea. Note that, the 670 cm^{-1} peak appeared at the temperature of 300 ℃ while the 1101 cm^{-1} disappeared at the same temperature, confirming that the urea reacted with water under the temperature of 300 ℃. Moreover, the above reaction generated reducibility gas of NH_3, which would induce layered MoO_3 to produce MoO_{3-x}. In our present work, the reaction between NH_3 and layered MoO_3 with the suitable molar ratios under the temperature of 550 ℃, the $N-MoO_2$ was produced with the unchanged layered morphology; when the temperature was up to 580 (~600) ℃, the morphology was changed into nano-particles (Fig. S5). To our best knowledge, it was the first time to report the synthesis of N doped MoO_2 nanosheet with the detecting pathways.

The detailed structure of studied $N-MoO_2$ sample should be studied for the next HER application. Table S1 shows the molar ratio of N to O element through three different measurements i.e. XPS, SEM-EDS and ICP. All results confirms that the atomic ratio of doped N element to oxygen is ca. 1:9. That is, one of the ten oxygen atoms in MoO_2 has been replaced by foreign nitrogen. Such a new MoO_2 sample should be expected to own the excellent catalytic activity, owing to the extraordinary or novel features of surface N doping, surface disordered space lattice and 2-D sheet structure. In electrocatalytic HER, proton migration and adsorption with the corresponding desorption binding energy are crucial and have been confirmed to interrelate with the surface state.[27, 38-40]

2.2 HER performance of N-MoO₂ nanosheets

With above interesting and promising results in hand, we next moved to the HER measurements. The HER electrocatalytic performance of the samples under study was carried out in 0.5 M H_2SO_4 using a typical three-electrode setup and the Ag/AgCl and graphite rod were chosen for reference and counter electrode, respectively. The catalysts were coated on glass carbon (GC) (Experimental section) for the use as working electrode. For comparison, the HER activity measurements of commercial 20% Pt/C, MoO_2 and MoO_3 were also carried out. As shown in **Fig. 4**(a), all the samples exhibit the *iR*-corrected reduction current response under the electrode potential range from 0.8 to 0 V (vs RHE). Typically, the sample of commercial 20% Pt/C exhibited a small overpotential (η) value of 27 mV at the current density of 10mAcm[-2], similar to the reported literatures.[32-34] The bare MoO_3 sample showed the lowest catalyzed HER with the potential of 448 mV at 10 mA/cm^{2}, meanwhile, the MoO_2 and $N-MoO_2$ samples gave the 238 and 96 mV at that current, respectively, suggesting that the foreign non-noble element doping (here is N) was helpful for the HER performance.[16, 41-43] The HER reaction in acidic
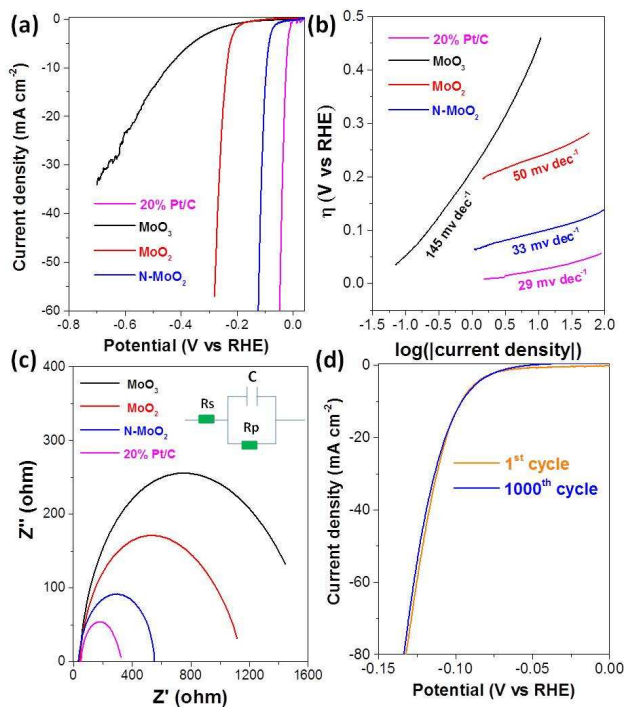
Fig. 4. Electrochemical HER measurements (iR corrected) of catalysts under study, 0.5M H_2SO_4 was used as the electrolyte. (a) Polarization curves and (B) corresponding Tafel plots of the $N-MoO_2$, MoO_2, MoO_3 and 20% Pt/C, recorded on glassy carbon electrodes, the catalyst loading was 0.2mg/cm^{2}, the scan rate was 20 mv/s; (c) electrochemical impedance spectra (EIS), the inset is the equivalent circuit; (d) Durability test for the N-MoO_2 catalyst, no obvious HER activity was lost after 1000 cycles.

solution can achieve according to different reaction intermediates and kinetic. To evaluate the HER kinetics of the studied MoO_2-based samples, the linear portion of the Tafel plots was fitted using the Tafel equation, $\eta = b \log j + a$, where j was the current density and b was the Tafel slope, and **Fig. 4**(b) showed the corresponding results. Clearly, the sample of Pt/C showed the smallest Tafel slope with the value of 29 mV dec[-1], whereas the other samples i.e. MoO_3, MoO_2 and $N-MoO_2$ exhibited 145, 50 and 33 mV dec[-1], respectively. There are two accepted mechanisms about the electrocatalytic hydrogen evolution, i.e. Volmer–Tafel mechanism (Tafel slope is less than or equal to 30 mV dec[-1]) with the recombination step rate-limiting and the Volmer–Heyrovsky mechanism (Tafel slope is great than or equal to 40 mV dec[-1]) with electrochemical desorption step rate-limiting. For the $N-MoO_2$ sample, the relative small Tafel slope suggests the Volmer–Tafel mechanism for the HER process. Two protons are adsorbed by the catalyst, and then they put together to generate hydrogen, the latter step determines the finial efficiency. It should be mentioned that the performance of synthesized sample is higher than other MoO_2-based samples in the literatures (see the comparison result in Table S2). Figure S12 gives the determination of the onset potential of the $N-MoO_2$ sample. The electrochemical impedances of studied samples were further measured by the electrochemical impedance spectroscopy (EIS) to indicate the fast electrode reaction kinetics. **Fig. 4**(c) showed the results

and the inset shows the corresponding equivalent circuit, where Rs represents the uncompensated resistance, Rp represents the charge transfer resistance and C shows the value of the argument of the constant phase element. We only pay attention to the relative resistance of the studied samples and the fitting results for Rs, Rp and C are not given here. As shown in **Fig. 4**(c), the Pt/C sample gives the smallest radius of circle, followed by $N-MoO_2$ nanosheet, reference MoO_2 and MoO_3, suggesting the relative fast electron transfer during HER for $N-MoO_2$, this consistent with the above polarization curves. The low overpotential, fast proton transformation with the low carrier migration resistance codetermine the high HER performance. In addition, the electrochemical stability of a catalyst is a nonnegligible parameter and then we tested the chronopotentiometry of the $N-MoO_2$ nanosheet sample. As shown in **Fig. 4**(d), the polarization curve after 1000 cycles test shows the ignorable negative shift compared with the initial one. To test the kinetic stability of the $N-MoO_2$ sample, the EIS compare measurements before and after durability test were also carried out as shown in Figure S13. No obvious change can be detected from the EIS curves, suggesting the excellent kinetic stability of the studied sample. And also we tested the I-t response under the constant voltage of 96 mV during the ~11 h. Figure S14 shows the corresponding result without obvious activity declining. And the inset in Figure S14 presents the direct H_2 generation bubbles during the electrocatalytic process during the reaction 2 s, the increased bubble indirectly indicate the fast reaction rate.

To understand well about the internal mechanism of N doping in MoO_2 lattice for improving HER performance, we tried to measure the double-layer capacitance (C_{dl}) of the $N-MoO_2$ and reference MoO_2. The C_{dl} can be derived from the cyclic voltammogrametry measurements with the different scan rates, and is thought to be proportional to the effective electrochemically active surface area (ECSA).[44-45] As shown in Fig. S15, the calculated C_{dl} values were 3 and 1.6 mF/cm^2 for $N-MoO_2$ and MoO_2, respectively. The large Cdl value of $N-MoO_2$ (almost twice over bare MoO_2) clearly indicates the high exposure of the active sites. The surface areas based on nitrogen desorption and adsorption are also shown in Figure S16 with the results of 52 and 46 m^2/g for $N-MoO_2$ and MoO_2, respectively. Bothe the ECSA and surface areas values suggest the more reaction sites of $N-MoO_2$ than MoO_2. As we discussed above, both MoO_2 and $N-MoO_2$ have the 2-D nanosheet morphology with the similar specific surface area, more exposed reaction sites are derived from the N doping. That is, N doping can introduce more reaction sites, such as proton adsorption, desorption and transfer sites, and then induce the efficient HER performance.

2.3 Mechanism analysis for $N-MoO_2$ HER performance

In the particular case of hydrogen evolution from electrocatalytic water splitting, there are two generally accepted mechanisms, i.e. Volmer–Heyrovsky and Volmer–Tafel reactions as shown in Fig. S17. The first step of two
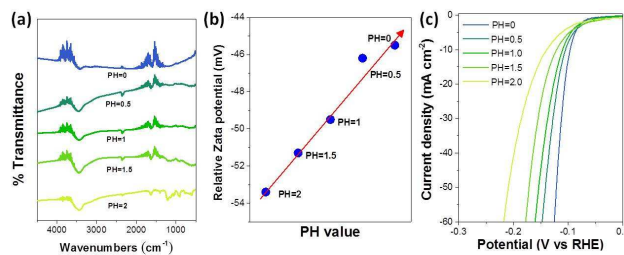
Fig. 5. Surface status analysis and the corresponding HER performance of the $N-MoO_2$ sample treated in the acid solution with different PH (0, 0.5, 1, 1.5 and 2). (a) IR spectra, (b) zeta potential plots and (c) LSV curves after *iR* correction.

protons being absorbing on the catalyst surface of the two mechanisms is same. And the following processes are different. Typically, in the case of Volmer–Heyrovsky, the absorbed proton and one new H$^+$ are combined with one electron to generate H_2; meanwhile, the two neighbour absorbed protons finish the reaction of releasing one H_2 molecule.[46-49] The strength of the hydrogen–metal bond formed at the first stage is believed and accepted to be important.[49] If the strength of the intermediates bind is too weak, the next steps of activating them become hard; if too strong, the available surface sites will be occupied with the undesired result of poisoning the reaction. Thus, it is reasonable to have one proper free energy of proton adsorption for the efficient HER performance. For the nitrogen element, it owns one unoccupied molecular orbital when replacing the oxygen element and the relative lower electronegativity than oxygen. Moreover, when it replaces one surface oxygen in one oxide, the disordered surface lattice, which can weak the proton adsorption bonds will be induced owing the different atomic radius. In the present N doped MoO_2 nanosheet sample, the internal mechanism for the excellent and enhanced HER should be discussed more according to experimental means and theoretical calculation.

To check the surface condition, five different strong acid solutions with the PH = 0, 0.5, 1, 1.5 and 2, were employed. The $N-MoO_2$ sample was treated via ultrasound ca. 30min in the acid solution and then vacuum drying for the following measurements. We first confirmed the proton adsorption of the surface sites through the Fourier Transform infrared spectroscopy (FTIR) measurements. In **Fig. 5**(a), the obvious different IR curves can be found. Typically, the IR peaks of absorbed water loaded at ca. 1640 and 3710 cm^{-1} are increasing from PH=2 to 0, and these peaks can be assigned to the vibration absorption of N-H, meanwhile, the intensity of the peak of adsorbed water at 1600 cm^{-1} is almost the same for the five samples, suggesting that more protons are adsorbed in the strong acid solution. Figure S18 gave the FTIR spectra of pristine $N-MoO_2$ sample with no visible 3710 cm^{-1} peak. Furthermore, the alkaline treated FTIR features were also shown in Figure S18b, no clear change compared with pristine $N-MoO_2$ sample can be detected, confirming the formation of N-H bond. We next tested the surface relative Zeta potential of the samples treated by different acid strong as shown in **Fig. 5**(b). Clearly, the potential plots change as a

ARTICLE
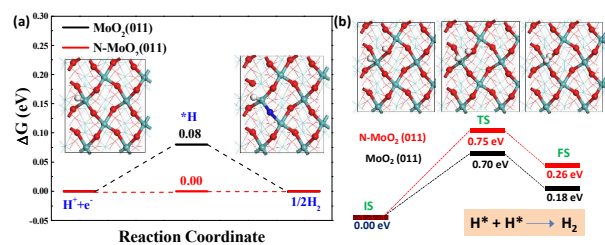
Fig. 6. DFT calculation studies for the HER processes. (a) Reaction pathway of adsorption and desorption of free energy (△G) of Volmer reaction; (b) the detailed activation and reaction processes of the HER processes.

linear function of PH value. In detail, when reducing the PH value, the Zeta potential increases, further suggesting that the more protons have been adsorbed by the surface sites of N-MoO_2 in the strong acid solution. Combining with the FTIR results, the N element doping indeed increases the proton absorbing sites and then answers the efficient and considerable Pt-like HER performance. It should be mentioned that the HER process of the N-MoO_2 sample follows the Volmer–Tafel route (**Fig. 4**), which requires two neighboring absorbed protons to achieve hydrogen evolution. On the sample of N doped MoO_2, the N doping sites work as one proton adsorption site with the nearby oxygen atom as the other site, the disordered surface lattices or crystal structure will lower the hydrogen–metal bond strength and then release the H_2 bubbles. Then, we tested the HER performance for verifying the assumption or deduction as given in **Fig. 5**(c). The sample of N-MoO_2 shows the gradual decreasing HER performance with the increasing PH value.

The extensive first-principle density functional theory (DFT) calculations were carried out to check the internal cause for the excellent HER performance of N-MoO_2 sample as given in **Fig. 6**. Owing to the chemical desorption (Tafel) process was the step-determined step for HER, the H atom Gibbs free energy of adsorption (△G) was first done and the result was shown in **Fig. 6**(a). For MoO_2, the surface unsaturated Mo atoms were the H adsorption sites and the △G was calculated to be 0.08 eV, while for N-MoO_2, the value was close to 0 eV, this result suggested that the replacement of N atoms to O atoms induced the increase of adsorptivity of Mo atoms. The herein low △G value of N-MoO_2 would boost the HER-active sites. The Tafel process (two H-adsorbed atoms close together to generate H_2) was then examined by also DFT. The corresponding activation and reaction processes were shown in **Fig. 6**(b). DFT calculations suggested that two adjacent adsorbed H was the incipient stage (IS) and the two H atoms approached each other was the corresponding transition state (TS), with the two H atoms combined together to generate H_2 as the final state (FS). Note that, the calculated activation barrier values of 0.7 eV for MoO_2 while 0.75 eV for N-MoO_2, existed a slight difference of 0.05eV, which had a nonsignificant effect on the final HER performance compared to adsorption and desorption of free energy (△G), and the two roles together led to the high HER performance of N-MoO_2 catalyst. Furthermore, the N-doped MoO_2 (011) model with an

oxygen defect was also built. The corresponding DFT results can be found in Figure S19. Clearly, for H adsorption on the N-doped MoO_2(011) with an oxygen atom defect, the first hydrogen tends to adsorb on the unsaturated Mo atom with a large adsorption Gibbs free energy of -0.88 eV. After that, it will decrease to -0.08 eV while the second hydrogen adsorbed on the N sites, which is the most balanced site for hydrogen evolution reaction. Thus, by comparison of hydrogen adsorption free energy on three model, the introduction of N doping on MoO_2(011) with and without defects is an effective method to enhance the HER performance.

2.4 Strategy expansion to Ni and Co systems

Our above results provide one new and stable nitrogen doped oxide (MoO_2) with the excellent electrocatalytic water splitting to hydrogen evolution performance. The other key aspect of above work is the synthesis strategy taking use of the oxide and cheap urea. The preparation process only needs Ar (O_2-free) atmosphere to finish the reduction reaction with the controllable products. To our best knowledge, it is the first time to synthesize MoO_2-based sample via the developed simple, reproducible and controlled method. The expansion or development of one strategy is vital to meet the need of large-scale preparation of samples. We next moved this method to other systems i.e. Ni and Co oxides. We chose the hydroxides ($Ni(OH)_2$ and $Co(OH)_x$) as the precursors. The mixtures with a certain ratios of hydroxides to urea were treated under the Ar condition at a certain temperature. In the case of Ni sample, a core-shell structure with nitrogen doped NiO and metal Ni was obtained and the XRD patterns were shown in Fig. S20(a). Without the adding of urea, only NiO/Ni was synthesized. Fig. S20(b) gave the corresponding TEM image of N-NiO/Ni sample with the clear core-shell result. XPS measurements in Fig. S21 further confirmed the formation of N-NiO/Ni. The corresponding electrocatalytic water splitting performance in Fig. S21(c) showed the enhanced HER activity of the N doped NiO/Ni sample compared to bare NiO/Ni. In the case of Co, the similar results can be found, i.e. XRD pattern in Fig. S22(a) with the CoO/Ni peaks, TEM image in Fig. S22(b) showing the core-shell structure, XPS results in Fig. S23(a) and (b) suggesting the N doped CoO and metal Co formation and the enhanced HER performance in Fig. S23(c). To further confirm the enhancement of HER performance of the N doped oxide/metal samples comes from the surface N doping, the samples of synthesized oxide/metal were treated by urea under the calcination temperature of 550 °C (N-MoO/M-1). Figure S24a shows the N 1s XPS spectra, suggesting the successful surface N doping. And according to the Figure S24b and c, all the N doped samples show the promoted HER curves, confirming the nitrogen boosted the improvement. All in all, the developed and reported method can be used to synthesize nitrogen doped oxides with the enhanced catalytic activity.

3. Conclusions

In summary, we have synthesized a new N-MoO$_2$ sheet sample with the excellent stable Pt-like HER performance. One simple and repeatable strategy is developed with the considerable wide applicability taking use of cheap, simple small organic molecule urea as the reducing agent. The outstanding electrocatalytic activity of the surface N element doping was detailed checked by utilizing XRD, XPS, TEM and EIS, as well as the surface state analysis i.e. FTIR and Zeta potential measurement. These comprehensive characterization methods conclusively show that the N doping can induce the disordered surface lattice, which will serves as the key role in determining the adsorption and desorption processes during HER, and also increase the proton adsorption sites with the relative weak binding force. Due to the cooperative effects of surface N doping, disordered surface distortion and also the intrinsic nature of MoO$_2$, the high and considerable HER activity can be obtained on the studied N-MoO$_2$ nanosheet sample with the activity of η = 96 mV vs RHE for the current density of −10 mA·cm^{-2}, a Tafel slope of 33 mV per decade, and a twice higher electrochemically active surface area than bare MoO$_2$ nanosheet. The detailed binding energy values in XPS spectra for the MoO$_2$ and MoO$_3$ are also systematic studied. Moreover, we further expanded the synthesis method to Ni and Co systems with the N-NiO/Ni and N-CoO/Co core-shell structures formation and they presented the enhanced HER performance compared to bare MO/M (M=metal) samples. This study provides new insights of N doing into one oxide for the catalytic activity, and also can help us design new Earth-abundant electrocatalysts or photocatalysts with further enhanced catalytic performance.

4. Experimental Section

Materials synthesis: A modified gas-solid reaction was used to fabricate N-MoO$_2$ samples by using corresponding solid precursors (MoO$_3$·nH$_2$O and urea). Typically, the accurate weighing of MoO$_3$·nH$_2$O and urea was added into one quartz mortar with the following grinding thoroughly. The mixture was transferred to one crucible with one same crucible as the cover. Then, the mixture was thermal treated by a certain temperature under the flowing Ar atmosphere. Note that, the heating rate was set to be 1˚C/min to ensure sufficient gas-solid reaction.

Material characterization: Transmission electron microscopy (TEM) test was performed on a FEI Tecnai G2 F20 electron microscope at an acceleration voltage of 200 kV. The field emission scanning electron microscopy (FESEM) were observed under a SU8020 electron microscopy. X-ray diffraction (XRD) patterns of the samples were recorded on a Rigaku Smartlab-9kW instrument using Cu Kα X-ray (λ = 1.54186 Å) radiation at a scanning rate of 4 ^{o}/min in the region of 2θ = 10-80°. X-ray photoelectron spectra (XPS) were acquired on a Kratos Axis Ultra DLD spectrometer with Al Kα (*hυ* = 1486.6 eV) as the excitation source. Fourier transform infrared reflectance (FTIR) and the Quasi FTIR spectra of

samples were carried out on a Bruker V70 spectrometer with a Pike heat chamber. The electrocatalytic water splitting performances were carried out in a conventional three-electrode cell on a Zennium Zahner electrochemical workstation. The Ag/AgCl (saturated KCl) and graphite rod were used as the reference and counter electrode, respectively. The measured potentials vs. Ag/AgCl were converted to the reversible hydrogen electrode (RHE) scale according to the following Nernst equation:

$E_{RHE} = E_{Ag/AgCl} + 0.059 \text{ pH} + E^o_{Ag/AgCl}$

where E_{RHE} is the converted potential vs. RHE, $E^o_{Ag/AgCl}$ = 0.1976 at 25 °C, and $E_{Ag/AgCl}$ is the experimentally measured potential against Ag/AgCl reference. For the 0.5M H$_2$SO$_4$ solution, the PH=0.3 at 25 °C, and then the calibration process can be written as: $E_{RHE} = E_{Ag/AgCl} + 0.2513$

DFT calculations: Density functional theory modeling of hydrogen adsorption on the surface of MoO$_2$ was optimized by Vienna Ab initio simulation package.[50] Projector augmented wave with generalized gradient approximation of PBE exchange-correlation functional[51] was adopted to optimize the ground electronic and ionic properties of the system until the convergence criteria of energy (10-4 eV) and force (0.05 eV/Å) were met. The cut-off energy 400 eV with a Gaussian smearing 0.05 eV was used for the (2×2) slab model of MoO$_2$ (011) with five layers. Then a vacuum layer of 15Å was built to avoid the layer coupling.

The adsorption of hydrogen on the MoO$_2$ was calculated as

$E(*H) = E(*H@MoO_2) − E(MoO_2) − ½ E(H_2)$

Where $E(*H@MoO_2)$ and $E(MoO_2)$ are the total energies of MoO$_2$(011) with and without hydrogen adsorption and the $E(H_2)$ is the total energy of hydrogen molecule. Further, the Gibbs free energy of hydrogen adsorption is corrected with a constant 0.24 eV at 298K, as previous reference reported.[52-53]

Conflicts of interest

There are no conflicts to declare.

Acknowledgements

References

1   J. A. Turner, *Science,* 2004, **305**, 972.

2   T. Zhang, M. Y. Wu, D. Y. Yan, J. Mao, H. Liu, W. B. Hu, X. W. Du, T. Ling and S. Z. Qiao, *Nano Energy,* 2018, **43**, 103.
3   N. S. Lewis and D. G. Nocera, *Proc. Natl. Acad. Sci. U. S. A.,* 2006, **103,** 15729.
4   Y. Zheng, Y. Jiao, A. Vasileff and S. Z. Qiao, *Angew. Chem. Int. Ed.,* 2018, DOI:10.1002/anie.201710556.
5   Y. Hou, B. L. Abrams, P. C. K. Vesborg, M. E. Björketun, K. Herbst, L. Bech, A. M. Setti, C. D. Damsgaard, T. Pedersen, O. Hansen, J. Rossmeisl, S. Dahl, J. K. Nørskov and I. Chorkendorff, *Nat. Mater.,* 2011, **10,** 434.
6   A. B. Laursen, S. Kegnaes, S. Dahl and I. Chorkendorff, *Energy Environ. Sci.,* 2012, **5,** 5577.
7   M. A. Lukowski, A. S. Daniel, C. R. English, F. Meng, A. Forticaux, R. J. Hamers and S. Jin, *Energy Environ. Sci.,* 2014, **7,** 2608.
8   B. Song and S. Jin, *Joule,* 2017, **1,** 220.
9   J. Kibsgaard, Z. Chen, B. N. Reinecke and T. F. Jaramillo, *Nat. Mater.,* 2012, **11,** 963.
10   Y. Yin, J. Han, Y. Zhang, X. Zhang, P. Xu, Q. Yuan, L. Samad, X. Wang, Y. Wang, Z. Zhang, P. Zhang, X. Cao, B. Song and S. Jin, *J. Am. Chem. Soc.,* 2016, **138,** 7965.
11   Y. Zhao, C. Chang, F. Teng, Y. Zhao, G. Chen, R. Shi, G. I. N. Waterhouse, W. Huang and T. Zhang, *Adv. Energ. Mater.,* 2017, **7,** 1700005.
12   S. Deng, Y. Zhong, Y. Zeng, Y. Wang, Z. Yao, F. Yang, S. Lin, X. Wang, X. Lu, X. Xia and J. Tu, *Adv. Mater.,* 2017, **29,** 1700748..
13   B. Liu, Y.-F. Zhao, H.-Q. Peng, Z.-Y. Zhang, C.-K. Kit Sit, M.-F. Yuen, T.-R. Zhang, C.-S. Lee and W.-J. Zhang, *Adv. Mater.,* 2017, **29,** 1606521.
14   T. F. Jaramillo, K. P. Jørgensen, J. Bonde, J. H. Nielsen, S. Horch and I. Chorkendorff, *Science,* 2007, **317,** 100.
15   X. Zhao, X. Ma, J. Sun, D. Li and X. Yang, *ACS Nano,* 2016, **10,** 2159.
16   J. Yan, H. Wu, P. Li, H. Chen, R. Jiang and S. (Frank) Liu, *J. Mater Chem A,* 2017, **5,** 10173.
17   J. Xiong, J. Li, J. Shi, X. Zhang, N.-T. Suen, Z. Liu, Y. Huang, G. Xu, W. Cai, X. Lei, L. Feng, Z. Yang, L. Huang and H. Cheng, *ACS Energy Lett,* 2018, **3,** 341.
18   M.-S. Balogun, Y. Huang, W. Qiu, H. Yang, H. Ji and Y. Tong, *Mater. Today,* 2017, **20,** 425.
19   M.-S. Balogun, W. Qiu, Y. Huang, H. Yang, R. Xu, W. Zhao, G.-R. Li, H. Ji and Y. Tong, *Adv. Mater.*, 2017, **29,** 1702095.
20   T. Kou, T. Smart, B. Yao, I. Chen, D. Thota, Y. Ping and Y. Li, *Adv. Energy Mater.*, 2018, DOI: 10.1002/aenm.201703538.
21   M.-S. Balogun, W. Qiu, H. Yang, W. Fan, Y. Huang, P. Fang, G. Li, H. Ji and Y. Tong, *Energy Environ. Sci.*, 2016, **9,** 3411.
22   H. Yan, Y. Xie, Y. Jiao, A. Wu, C. Tian, X. Zhang, L. Wang and H. Fu, *Adv. Mater.,* 2018, **30,** 1704156.
23   J. Jeon, Y. Park, S. Choi, J. Lee, S. S. Lim, B. H. Lee, Y. J. Song, J. H. Cho, Y. H. Jang and S. Lee, *ACS Nano,* 2018, **12,** 338.
24   J. Zhang, T. Wang, P. Liu, Z. Liao, S. Liu, X. Zhuang, M. Chen, E. Zschech and X. Feng, *Nat. Commun.,* 2017, **8,** 15437.
25   H. Park, A. Encinas, J. P. Scheifers, Y. Zhang and B. P. T. Fokwa, *Angew. Chem., Int. Ed.,* 2017, **56,** 5575.
26   H. Park, Y. Zhang, J. P. Scheifers, P. R. Jothi, A. Encinas and B. P. T. Fokwa, *J. Am. Chem. Soc.,* 2017, **139,** 12915.
27   M. Qamar, A. Adam, B. Merzougui, A. Helal, O. Abdulhamid and M. N. Siddiquib, *J. Mater. Chem. A,* 2016, **4,** 16225.
28   H. Lin, Z. Shi, S. He, X. Yu, S. Wang, Q. Gao and Y. Tang, *Chem. Sci.,* 2016, **7,** 3399.
29   Y.-Y. Chen, Y. Zhang, X. Zhang, T. Tang, H. Luo, S. Niu, Z.-H. Dai, L.-J. Wan and J.-S. Hu, *Adv. Mater.,* 2017, **29,** 1703311.
30   Z. Luo, R. Miao, T. Doan, H. Islam, M. Mosa, A. S. Poyraz, W. Zhong, J. E. Cloud, D. A. Kriz, S. Thanneeru, J. He, Y. Zhang, R. Ramprasad and S. L. Suib, *Adv. Energ. Mater.,* 2016, **6,** 1600528.

31   R. S. Datta, F. Haque, M. Mohiuddin, B. J. Carey, N. Syed, A. Zavabeti, B. Zhang, H. Khan, K. J. Berean, J. Z. Ou, N. Mahmood, T. Daeneke and K. Kalantar-zadeh, *J. Mater. Chem. A,* 2017, **5,** 24223.
32   Y.-J. Tang, M.-R. Gao, C.-H. Liu, S.-L. Li, H.-L. Jiang, Y.-Q. Lan, M. Han and S.-H. Yu, *Angew. Chem., Int. Ed.,* 2015, **54,** 12928.
33   P. Jiang, Y. Yang, R. Shi, G. Xia, J. Chen, J. Su and Q. Chen, *J. Mater. Chem. A,* 2017, **5,** 5475.
34   Y. Jin, H. Wang, J. Li, X. Yue, Y. Han, P. K. Shen annd Y. Cui, *Adv. Mater.,* 2016, **28,** 3785.
35   X. Chen, G. Liu, W. Zheng, W. Feng, W. Cao, W. Hu and P. Hu, *Adv. Funct. Mater.,* 2016, **26,** 8537.
36   X. Xie, R. Yu, N. Xue, A. B. Yousaf, H. Du, K. Liang, N. Jiang and A.-W. Xu, *J. Mater. Chem. A,* 2016, **4,** 1647.
37   H. Bian, Y. Ji, J. Yan, P. Li, L. Li, Y. Li and S. (Frank) Liu, *Small,* 2018, **14,** 1703003.
38   Z. Zhuang, Y. Li, Z. Li, F. Lv, Z. Lang, K. Zhao, L. Zhou, L. Moskaleva, S. Guo and L. Mai, *Angew. Chem., Int. Ed.,* 2018, **57,** 496.
39   M. R. Nellist, F. A. L. Laskowski, J. Qiu, H. Hajibabaei, K. Sivula, T. W. Hamann and S. W. Boettcher, *Nat. Energy,* 2018, **3,** 46.
40   Y. Jiao, Y. Zheng, K. Davey and S.-Z. Qiao, *Nat. Energy,* 2016, **1,** 16130.
41   K. Qu, Y. Zheng, X. Zhang, K. Davey, S. Dai and S.-Z. Qiao, *ACS Nano,* 2017, **11,** 7293.
42   H. Fei, J. Dong, M. J. Arellano-Jiménez, G. Ye, N. D. Kim, E. L.G. Samuel, Z. Peng, Z. Zhu, F. Qin, J. Bao, M. J. Yacaman, P. M. Ajayan, D. Chen and J. M. Tour, *Nat. Commun.,* 2015, **6,** 8668.
43   H. Wang, Q. Yi, L. Gao, Y. Gao, T. Liu, Y.-B. Jiang, Y. Sun and G. Zou, *Nanoscale,* 2017, **9,** 16342.
44   J. Zhuo, M. Cabán-Acevedo, H. Liang, L. Samad, Q. Ding, Y. Fu, M. Li and S. Jin, *ACS Catal.,* 2015, **5,** 6355.
45   C. Xia, H. Liang, J. Zhu, U. Schwingenschlögl and H. N. Alshareef, *Adv. Energy Mater.,* 2017, **7,** 1602089.
46   Y. Zheng, Y. Jiao, Y. Zhu, L. H. Li, Y. Han, Y. Chen, A. Du, M. Jaroniec and S.-Z. Qiao, *Nat. Commun.,* 2014, **5,** 3783.
47   T. Ling, D.-Y. Yan, H.Wang, Y. Jiao, Z. Hu, Y. Zheng, L. Zheng, J. Mao, H.Liu, X.-W. Du, M. Jaroniec and S.-Z. Qiao, *Nat. Commun.,* 2017, **8,** 1509.
48   D. Voiry, H. Yamaguchi, J. Li, R. Silva, D. C. B. Alves, T. Fujita, M. Chen, T. Asefa, V. B. Shenoy, G. Eda and M. Chhowalla, *Nat. Mater.,* 2013, **12,** 850.
49   J. Greeley, T. F. Jaramillo, J. Bonde, I. Chorkendorff and J. K. Nørskov, *Nat. Mater.,* 2006, **5,** 909.
50   G. Kresse and J. Furthmüller, *Phys. Rev. B,* 1996, **54,** 11169.
51   J. P. Perdew, K. Burke and M. Ernzerhof, *Phys. Rev. Lett.,* 1996, **77,** 3865.
52   Q. Tang and D. E. Jiang, *ACS Catal.,* 2016, **6,** 4953.
53   B. C. Wood, E. Schwegler and T. Ogitsu, *Adv. Energ. Matter.,* 2015, **5,** 1501423.

TOC
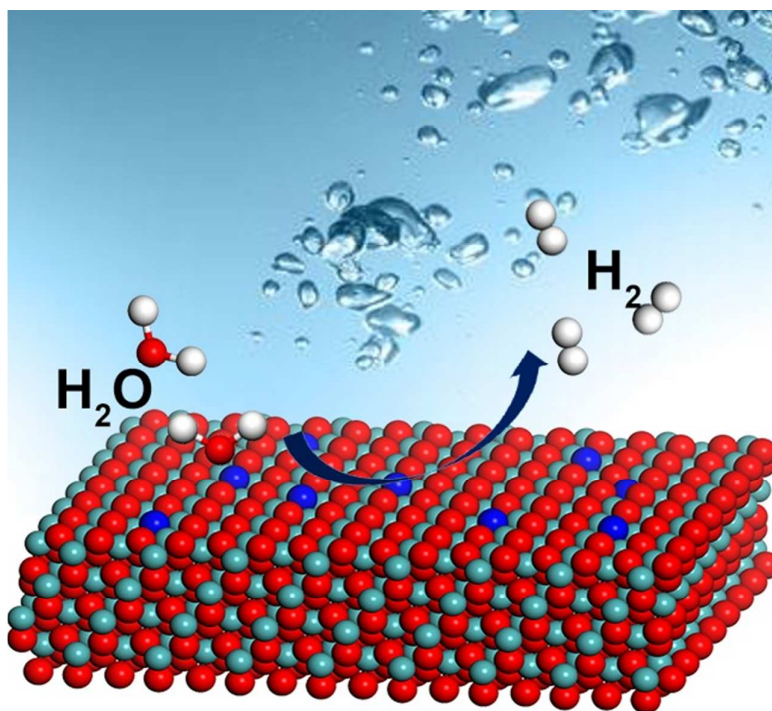
One simple and repeatable strategy is developed to synthesize N-MoO_2 nanosheet

with the excellent stable Pt-like HER performance.